

Strongly correlated Fermi-systems: non-Fermi liquid behavior, quasiparticle effective mass and their interplay

V.R. Shaginyan,^{1,2,*} M.Ya. Amusia,² and K.G. Popov³

¹*Petersburg Nuclear Physics Institute, RAS, Gatchina, 188300, Russia*

²*Racah Institute of Physics, Hebrew University, Jerusalem 91904, Israel*

³*Komi Science Center, Ural Division, RAS, Syktyvkar, 167982, Russia*

Basing on the density functional theory of fermion condensation, we analyze the non-Fermi liquid behavior of strongly correlated Fermi-systems such as heavy-fermion metals. When deriving equations for the effective mass of quasiparticles, we consider solids with a lattice and homogeneous systems. We show that the low-temperature thermodynamic and transport properties are formed by quasiparticles, while the dependence of the effective mass on temperature, number density, magnetic fields, etc gives rise to the non-Fermi liquid behavior. Our theoretical study of the heat capacity, magnetization, energy scales, the longitudinal magnetoresistance and magnetic entropy are in good agreement with the remarkable recent facts collected on the heavy-fermion metal YbRh₂Si₂.

PACS numbers: 71.27.+a, 76.60.Es, 73.43.Qt

Keywords: Quantum criticality; Heavy-fermion metals; Energy scales; Magnetoresistance; Magnetic entropy

I. INTRODUCTION

The Landau theory of Fermi liquids has a long history and remarkable results in describing the properties of electron liquid in ordinary metals and Fermi liquids of ³He type. The theory is based on the Landau paradigm that elementary excitations determine the physics at low temperatures. These excitations behave as quasiparticles, have a certain effective mass M^* , which is independent of temperature T , number density x , and magnetic field strength B and is a parameter of the theory [1]. The discovery of strongly correlated Fermi systems represented by heavy-fermion (HF) metals and 2D ³He exhibiting the non-Fermi liquid (NFL) behavior has opened tremendous challenges in the modern condensed matter physics [2, 3, 4, 5, 6]. Facts collected on HF metals and 2D ³He demonstrate that the effective mass strongly depends on T , x , B etc, while M^* itself can reach very high values or even diverge [4, 5]. Such a behavior is so unusual that the traditional Landau quasiparticles paradigm does not apply to it.

There is a common wisdom that quantum criticality, describing the collective fluctuations of matter undergoing a second-order phase transition at zero temperature, suppresses quasiparticles and thus generates the NFL behavior, depending on the initial ground state, either magnetic or superconductive [2, 3, 4, 5, 6]. Earlier, a concept of fermion condensation quantum phase transition (FCQPT) preserving quasiparticles and intimately related to the unlimited growth of M^* , had been suggested [7, 8]. Further studies show that it is capable to deliver an adequate theoretical explanation of vast majority of experimental results in different HF metals [9, 10, 11]. In contrast to the Landau paradigm based

on the assumption that M^* is a constant, in FCQPT approach M^* strongly depends on T , x , B etc. Therefore, in accord with numerous experimental facts the extended quasiparticles paradigm is to be introduced. The main point here is that the well-defined quasiparticles determine as before the thermodynamic and transport properties of strongly correlated Fermi-systems, while M^* becomes a function of T , x , B etc [10, 11, 12, 13]. The FCQPT approach had been already successfully applied to describe the thermodynamic properties of such different strongly correlated systems as ³He on one side and complicated heavy-fermion (HF) compounds on the other side [11, 12, 13, 14, 15, 16].

In this letter, we analyze the non-Fermi liquid behavior of strongly correlated Fermi systems using the density functional theory of fermion condensation [17]. We derive equations for the effective mass of quasiparticles in both homogeneous systems and solids with a lattice, and show that extended quasiparticles paradigm is valid, while the dependence of the effective mass on T , x , B etc gives rise to the NFL behavior. The obtained results are illustrated with calculations of the thermodynamic and transport functions of strongly correlated Fermi-systems. Possible energy scales in these functions are discussed. We demonstrate that our calculations of the heat capacity C/T , magnetization M , energy scales, longitudinal magnetoresistance (LMR) and magnetic entropy $S(B)$ are in good agreement with striking recent facts collected on the HF metal YbRh₂Si₂ [18, 19, 20].

II. EQUATION FOR THE EFFECTIVE MASS

At first, consider HF liquid at $T = 0$ characterized by the effective mass M^* . Upon applying well-known Landau equation, we can relate M^* to the bare electron

*Electronic address: vrshag@thd.pnpi.spb.ru

mass M [1, 21]

$$\frac{M^*}{M} = \frac{1}{1 - N_0 F^1(x)/3}. \quad (1)$$

Here N_0 is the density of states of a free electron gas, M is the bare mass, $x = p_F^3/3\pi^2$ is the number density, p_F is the Fermi momentum, and $F^1(x)$ is the p -wave component of Landau interaction amplitude F . When at some critical point $x = x_c$, $F^1(x)$ achieves certain threshold value, the denominator in Eq. (1) tends to zero so that the effective mass diverges at $T = 0$ [21], and the system undergoes FCQPT. It follows from Eq. (1) that beyond the critical point x_c , the effective mass becomes negative. To avoid an unstable and physically meaningless state with a negative effective mass, the system must undergo a quantum phase transition at the quantum critical point $x = x_c$, which is FCQPT [8, 10]. The asymmetrical phase behind the quantum critical point is determined by

$$\frac{\delta E}{\delta n(\mathbf{p})} = \mu, \quad (2)$$

here E is the ground state energy, μ is a chemical potential, and $n(\mathbf{p})$ is the occupation numbers of quasiparticles. The main result of such reconstruction is that instead of Fermi step, we have $0 \leq n(p) \leq 1$ in certain range of momenta $p_i \leq p \leq p_f$. Accordingly, the single-particle spectrum

$$\frac{\delta E}{\delta n(\mathbf{p})} = \varepsilon(\mathbf{p}), \quad (3)$$

in the above momenta interval becomes flat, $\varepsilon(\mathbf{p}) = \mu$, and this state is known as a fermi condensate (FC) state [7]. Due to the above peculiarities of the $n(\mathbf{p})$ function, FC state is characterized by the superconducting order parameter $\kappa(\mathbf{p}) = \sqrt{n(\mathbf{p})(1 - n(\mathbf{p}))}$.

To derive equation determining the effective mass, we employ the density functional theory of superconducting state [22]. In that case, the ground state energy E becomes the functional of the occupation numbers and the function of the number density x , $E = E[n(\mathbf{p}), x]$, while Eq. (3) gives the single-particle spectrum [17]. Upon differentiating the both sides of Eq. (3) with respect to \mathbf{p} and after some algebra and integration by parts, we obtain

$$\frac{\partial \varepsilon(\mathbf{p})}{\partial \mathbf{p}} = \frac{\mathbf{p}}{M} + \int F(\mathbf{p}, \mathbf{p}_1) \frac{\partial n(\mathbf{p}_1)}{\partial \mathbf{p}_1} \frac{d\mathbf{p}_1}{(2\pi)^3}. \quad (4)$$

Here, $F(\mathbf{p}, \mathbf{p}_1) = \delta^2 E / \delta n(\mathbf{p}) \delta n(\mathbf{p}_1)$ is the Landau amplitude. To calculate the derivative $\partial \varepsilon(\mathbf{p}) / \partial \mathbf{p}$, we employ the functional representation

$$E[n] = \int \frac{p^2}{2M} n(\mathbf{p}) \frac{d\mathbf{p}}{(2\pi)^3} + \frac{1}{2} \int F(\mathbf{p}, \mathbf{p}_1) n(\mathbf{p}) n(\mathbf{p}_1) \frac{d\mathbf{p} d\mathbf{p}_1}{(2\pi)^6} + \dots \quad (5)$$

It is seen directly from Eq. (4) that the effective mass is given by the well-known Landau equation

$$\frac{1}{M^*} = \frac{1}{M} + \int \frac{\mathbf{p}_F \mathbf{p}_1}{p_F^3} F(\mathbf{p}_F, \mathbf{p}_1) \frac{\partial n(p_1)}{\partial p_1} \frac{d\mathbf{p}_1}{(2\pi)^3}. \quad (6)$$

For simplicity, we ignore the spin dependencies. To calculate M^* as a function of T , we construct the free energy $F = E - TS$, where the entropy S is given by

$$S = -2 \int [n(\mathbf{p}) \ln(n(\mathbf{p})) + (1 - n(\mathbf{p})) \ln(1 - n(\mathbf{p}))] \frac{d\mathbf{p}}{(2\pi)^3}, \quad (7)$$

which follows from general combinatorial reasoning [1]. Minimizing F with respect to $n(\mathbf{p})$, we arrive at the Fermi-Dirac distribution,

$$n(\mathbf{p}, T) = \left\{ 1 + \exp \left[\frac{(\varepsilon(\mathbf{p}, T) - \mu)}{T} \right] \right\}^{-1}. \quad (8)$$

Due to the above derivation, we conclude that Eqs. (4) and (6) are exact ones and allow us to calculate the behavior of both $\partial \varepsilon(\mathbf{p}) / \partial \mathbf{p}$ and M^* in the vicinity of FCQPT where the well-defined quasiparticles determine the low-temperature physics, while M^* becomes a divergent function of T , B and x [10, 11, 12, 13]. As we will see this feature of M^* forms the NFL behavior observed in measurements on HF metals.

III. SCALING BEHAVIOR OF THE EFFECTIVE MASS

To avoid difficulties associated with the anisotropy generated by the crystal lattice of solids, we study the universal behavior of heavy-fermion metals using the model of the homogeneous heavy-electron (fermion) liquid. The model is quite meaningful because we consider the universal behavior exhibited by these materials at low temperatures, a behavior related to power-law divergences of quantities such as the effective mass, the heat capacity, the magnetization, etc. These divergences and scaling behavior of the effective mass, or the critical exponents that characterize them, are determined by energy and momentum transfers that are small compared to the Debye characteristic temperature and momenta of the order of the reciprocal lattice cell length a^{-1} . Therefore quasiparticles are influenced by the crystal lattice averaged over big distances compared to the length a . Thus, we can substitute the well-known jelly model for the lattice as it is usually done, for example, in the fluctuation theory of second order phase transitions.

The schematic phase diagram of HF liquid is reported in Fig. 1. Magnetic field B is taken as the control parameter. In fact, the control parameter can be pressure P or doping (the number density) x etc as well. At $B = B_{c0}$, FC takes place leading to a strongly degenerated state, where B_{c0} is a critical magnetic field, such that at $B > B_{c0}$ the system is driven towards its Landau Fermi liquid (LFL) regime. In our simple model B_{c0}

is a parameter. The FC state is captured by the superconducting (SC), ferromagnetic (FM), antiferromagnetic (AFM) etc. states lifting the degeneracy [10, 11]. Below we consider the HF metal YbRh_2Si_2 . In that case, $B_{c0} \simeq 0.06$ T ($B \perp c$) and at $T = 0$ and $B < B_{c0}$ the AFM state takes place [20]. At elevated temperatures and fixed magnetic field the NFL regime occurs, while rising B again drives the system from NFL region to LFL one as shown by the dash-dot horizontal arrow in Fig. 1. Below we consider the transition region when the system moves from NFL regime to LFL one along the horizontal arrow and it moves from LFL regime to NFL one along the vertical arrow as shown in Fig. 1. The inset to Fig. 1 demonstrates the behavior of the normalized effective mass $M_N^* = M^*/M_M^*$ versus normalized temperature $T_N = T/T_M$, where M_M^* is the maximum value that M^* reaches at $T = T_M$. The $T^{-2/3}$ regime is marked as NFL one since the effective mass depends strongly on temperature. The temperature region $T \simeq T_M$ signifies the crossover between the LFL regime with almost constant effective mass and NFL behavior, given by $T^{-2/3}$ dependence. Thus temperatures $T \sim T_M$ can be regarded as the crossover region between LFL and NFL regimes.

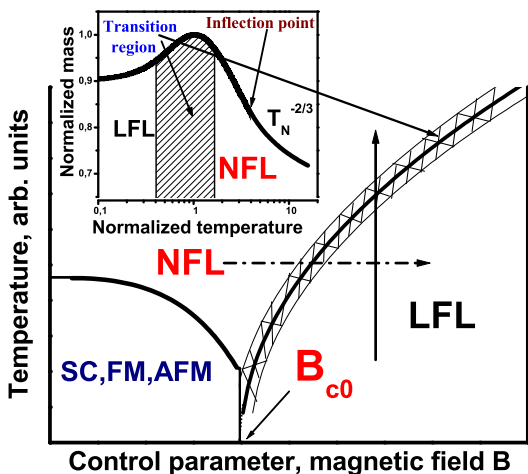


FIG. 1: Schematic phase diagram of HF metals. B_{c0} is magnetic field at which the effective mass divergences. SC, FM, AFM denote the superconducting (SC), ferromagnetic (FM) and antiferromagnetic (AFM) states, respectively. At $B < B_{c0}$ the system can be in SC, FM or AFM states. The vertical arrow shows the transition from the LFL regime to the NFL one at fixed B along T with M^* depending on T . The dash-dot horizontal arrow illustrates the system moving from NFL regime to LFL one along B at fixed T . The inset shows a schematic plot of the normalized effective mass versus the normalized temperature. Transition regime, where M_N^* reaches its maximum value M_M^* at $T = T_M$, is shown by the hatched area both in the main panel and in the inset. The arrows mark the position of inflection point in M_N^* and the transition region.

To explore a scaling behavior of M^* , we write the quasiparticle distribution function as $n_1(\mathbf{p}) = n(\mathbf{p}, T) - n(\mathbf{p})$, with $n(\mathbf{p})$ is the step function, and Eq. (6) then

becomes

$$\frac{1}{M^*(T)} = \frac{1}{M^*} + \int \frac{\mathbf{p}_F \mathbf{p}_1}{p_F^3} F(\mathbf{p}_F, \mathbf{p}_1) \frac{\partial n_1(p_1, T)}{\partial p_1} \frac{d\mathbf{p}_1}{(2\pi)^3}. \quad (9)$$

At FCQPT the effective mass M^* diverges and Eq. (9) becomes homogeneous determining M^* as a function of temperature

$$M^*(T) \propto T^{-2/3}, \quad (10)$$

while the system exhibits the NFL behavior [10, 13]. If the system is located before FCQPT, M^* is finite, at low temperatures the system demonstrates the LFL behavior that is $M^*(T) \simeq M^* + a_1 T^2$, with a_1 is a constant, see the inset to Fig. 1. Obviously, the LFL behavior takes place when the second term on the right hand side of Eq. (9) is small in comparison with the first one. Then, at rising temperatures the system enters the transition regime: M^* grows, reaching its maximum M_M^* at $T = T_M$, with subsequent diminishing. Near temperatures $T \geq T_M$ the last "traces" of LFL regime disappear, the second term starts to dominate, and again Eq. (9) becomes homogeneous, and the NFL behavior restores, manifesting itself in decreasing of M^* as $T^{-2/3}$. When the system is near FCQPT, it turns out that the solution of Eq. (9) $M^*(T)$ can be well approximated by a simple universal interpolating function [10, 13, 15]. The interpolation occurs between the LFL ($M^* \simeq M^* + a_1 T^2$) and NFL ($M^* \propto T^{-2/3}$) regimes thus describing the above crossover [10, 13]. Introducing the dimensionless variable $y = T_N = T/T_M$, we obtain the desired expression

$$M_N^*(y) \approx c_0 \frac{1 + c_1 y^2}{1 + c_2 y^{8/3}}. \quad (11)$$

Here $M_N^* = M^*/M_M^*$ is the normalized effective mass, $c_0 = (1 + c_2)/(1 + c_1)$, c_1 and c_2 are fitting parameters, parameterizing the Landau amplitude.

It is possible to transport Eq. (9) to the case of the application of magnetic fields [13, 15]. The application of magnetic field restores the LFL behavior so that M_M^* depends on B as

$$M_M^* \propto (B - B_{c0})^{-2/3}, \quad (12)$$

while

$$T_M \propto \mu_B (B - B_{c0}), \quad (13)$$

where μ_B is the Bohr magneton [10, 13, 15]. Employing Eqs. (12) and (13) to calculate M_M^* and T_M , we conclude that Eq. (11) is valid to describe the normalized effective mass in external fixed magnetic fields with $y = T/(B - B_{c0})$. On the other hand, Eq. (11) is valid when the applied magnetic field becomes a variable, while temperature is fixed $T = T_f$. In that case, as seen from Eqs. (10), (11) and (12), it is convenient to rewrite both the variable as $y = (B - B_{c0})/T_f$, and Eq. (13) as

$$\mu_B (B_M - B_{c0}) \propto T_f. \quad (14)$$

It follows from Eq. (11) that in contrast to the Landau paradigm of quasiparticles the effective mass strongly depends on T and B . As we will see it is this dependence that forms the NFL behavior. It follows also from Eq. (11) that a scaling behavior of M^* near FCQPT point is determined by the absence of appropriate external physical scales to measure the effective mass and temperature. At fixed magnetic fields, the characteristic scales of temperature and of the function $M^*(T, B)$ are defined by both T_M and M_M^* respectively. At fixed temperatures, the characteristic scales are $(B_M - B_{c0})$ and M_M^* . It follows from Eqs. (12) and (13) that at fixed magnetic fields, $T_M \rightarrow 0$, and $M_M^* \rightarrow \infty$, and the width of the transition region shrinks to zero as $B \rightarrow B_{c0}$ when these are measured in the external scales. In the same way, it follows from Eqs. (10) and (14) that at fixed temperatures, $(B_M - B_{c0}) \rightarrow 0$, and $M_M^* \rightarrow \infty$, and the width of the transition region shrinks to zero as $T_f \rightarrow 0$.

A few remarks are in order here. As we shall see in Subsections IV C and D, in some cases temperature or magnetic field dependencies of the effective mass or of other observable like the longitudinal magnetoresistance do not have "peculiar points" like maximum. The normalizations are to be performed in the other points like the inflection point shown in the inset to Fig. 1. Such a normalization is possible since it is established on the internal scales.

IV. NON-FERMI LIQUID BEHAVIOR IN YbRh_2Si_2

In what follows, we compute the effective mass and employ Eq. (11) for estimations of considered values. To obtain the effective mass $M^*(T, B)$, we solve Eqs. (8) and (9) with special form of Landau interaction amplitude, see Refs. [10, 13] for details. Choice of the amplitude is dictated by the fact that the system has to be in the FCQPT point, which means that first two p -derivatives of the single-particle spectrum $\varepsilon(\mathbf{p})$ should equal zero. Since first derivative is proportional to the reciprocal quasiparticle effective mass $1/M^*$, its zero (where $1/M^* = 0$ and the effective mass diverges) just signifies FCQPT. Zeros of two subsequent derivatives mean that the spectrum $\varepsilon(\mathbf{p})$ has an inflection point at Fermi momentum p_F so that the lowest term of its Taylor expansion is proportional to $(p - p_F)^3$ [13]. After solution of Eq. (9), the obtained spectrum had been used to calculate the entropy $S(B, T)$, which, in turn, had been recalculated to the effective mass $M^*(T, B)$ by virtue of well-known LFL relation $M^*(B, T) = S(B, T)/T$. We note that our calculations confirm the validity of Eq. (11).

A. Heat capacity and the Sommerfeld coefficient

Exciting measurements of $C/T \propto M^*$ on samples of the new generation of YbRh_2Si_2 in different magnetic

fields B up to 1.5 T [18] allow us to identify the scaling behavior of the effective mass M^* and observe the different regimes of M^* behavior such as the LFL regime, transition region from LFL to NFL regimes, and the NFL regime itself. A maximum structure in $C/T \propto M_M^*$ at T_M appears under the application of magnetic field B and T_M shifts to higher T as B is increased. The value of $C/T = \gamma_0$ is saturated towards lower temperatures decreasing at elevated magnetic field, where γ_0 is the Sommerfeld coefficient [18].

It follows from Section III, that the transition region corresponds to the temperatures where the vertical arrow in the main panel of Fig. 1 crosses the hatched area. The width of the region, being proportional to $T_M \propto (B - B_{c0})$ shrinks, T_M moves to zero temperature and $\gamma_0 \propto M^*$ increases as $B \rightarrow B_{c0}$. These observations are in accord with the facts [18].

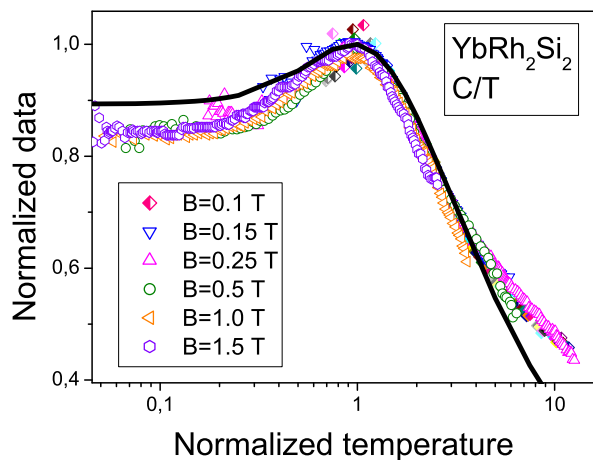


FIG. 2: The normalized effective mass M_N^* extracted from the measurements of the specific heat C/T on YbRh_2Si_2 in magnetic fields B shown in the left down corner [18]. Our calculations are depicted by the solid curve tracing the scaling behavior of M_N^* .

To obtain the normalized effective mass M_N^* , the maximum structure in C/T was used to normalize C/T , and T was normalized by T_M . In Fig. 2 the obtained M_N^* as a function of normalized temperature T_N is shown by geometrical figures, our calculations carried out as described above are shown by the solid line. Figure 2 reveals the scaling behavior of the normalized experimental curves - the curves at different magnetic fields B merge into a single one in terms of the normalized variable $y = T/T_M$. As seen from Fig. 2, the normalized mass M_N^* extracted from the measurements is not a constant, as would be for a LFL, and shows the scaling behavior given by Eq. (11) over three decades in normalized temperature. The two regimes (the LFL regime and NFL one) separated by the transition region, as depicted by the hatched area in the inset to Fig. 1, are clearly seen in Fig. 2 illuminating good agreement between the theory and facts.

B. “Average” magnetization

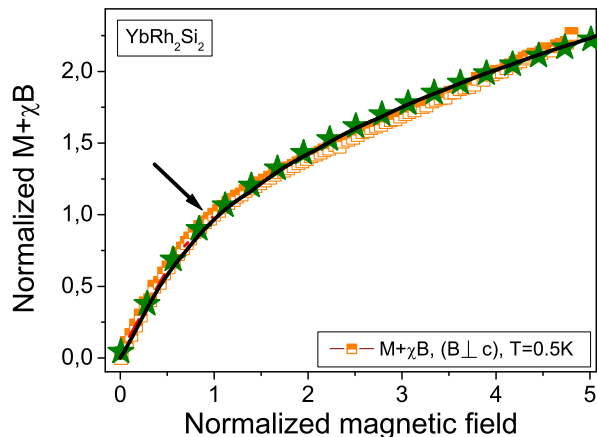


FIG. 3: The field dependence of the normalized “average” magnetization $\widetilde{M} \equiv M + B\chi$ is shown by squares and extracted from measurements collected on YbRu_2Si_2 [19]. The kink (shown by the arrow) is clearly seen at the normalized field $B_N = B/B_k \simeq 1$. The solid curve and stars (see text) represent our calculations.

Consider now an “average” magnetization $\widetilde{M} \equiv B\chi + M$ as a function of magnetic field B at fixed temperature $T = T_f$, where χ is the magnetic susceptibility and M is the magnetization,

$$M(B, T) = \int_0^B \chi(b, T) db, \quad (15)$$

where the magnetic susceptibility is given by [1]

$$\chi(B, T) = \frac{\beta M^*(B, T)}{1 + F_0^a}. \quad (16)$$

Here, β is a constant and F_0^a is the Landau amplitude related to the exchange interaction [1]. In the case of strongly correlated systems $F_0^a \geq -0.9$ [21]. Therefore, as seen from Eq. (16), due to the normalization the coefficients β and $(1 + F_0^a)$ drops out from the result, and $\chi \propto M^*$. To obtain \widetilde{M} , we calculate M^* as a function of B at fixed T_f . The obtained curves of \widetilde{M} exhibit energy scales separated by kinks at $B = B_k$. As seen from Fig. 3, the kink is a crossover point from the fast to slow growth of \widetilde{M} at rising magnetic field. We use B_k and $\widetilde{M}(B_k)$ to normalize B and \widetilde{M} respectively.

The normalized \widetilde{M} vs the normalized field $B_N = B/B_K$ are shown in Fig. 3. Our calculations are depicted by the solid line. The stars trace out our calculations of \widetilde{M} with $M^*(y)$ extracted from the data C/T shown in Fig. 2. The calculation procedure deserves a remark here. Namely, in that case M^* depends on $y = T/T_M$ with T_M is given by Eq. (13). On the other hand, we can consider $y = (B - B_{c0})/T_f$ as it is shown in Section III, and take the data C/T as a function of y .

It is seen from Fig. 3 that our calculations are in good agreement with the facts, and all the data exhibit the kink (shown by arrow) at $B_N \simeq 1$ taking place as soon as the system enters the transition region corresponding to the magnetic fields where the horizontal dash-dot arrow in the main panel of Fig. 1 crosses the hatched area. Indeed, as seen from Fig. 3, at lower magnetic fields \widetilde{M} is a linear function of B since M^* is approximately independent of B . It follows from Eq. (12) that at elevated magnetic fields M^* becomes a diminishing function of B and generates the kink in $\widetilde{M}(B)$ separating the energy scales discovered in Ref. [19]. Then, it seen from Eq. (14) that the magnetic field $B_k \simeq B_M$ at which the kink appears shifts to lower B as T_f is decreased.

C. Longitudinal magnetoresistance

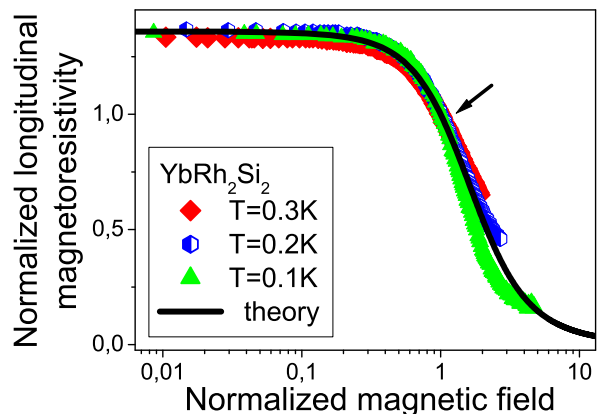


FIG. 4: Magnetic field dependence of the normalized (in the inflection point shown by the arrow, see text for details) magnetoresistance R_N^ρ versus normalized magnetic field. R_N^ρ was extracted from LMR of YbRh_2Si_2 at different temperatures [19] listed in the legend. The solid line represents our calculations.

Consider a longitudinal magnetoresistance (LMR) $\rho(B, T) = \rho_0 + AT^2$ as a function of B at fixed T_f . In that case, the classical contribution to LMR due to orbital motion of carriers induced by the Lorentz force is small, while the Kadowaki-Woods relation [23, 24], $K = A/\gamma_0^2 \propto A/\chi^2 = \text{const}$, allows us to employ M^* to construct the coefficient A [25], since $\gamma_0 \propto \chi \propto M^*$. As a result, $\rho(B, T) - \rho_0 \propto (M^*)^2$. Fig. 4 reports the normalized magnetoresistance

$$R_N^\rho(y) = \frac{\rho(y) - \rho_0}{\rho_{inf}} \propto (M_N^*(y))^2 \quad (17)$$

vs normalized magnetic field $y = B/B_{inf}$ at different temperatures, shown in the legend. Here ρ_{inf} and B_{inf} are LMR and magnetic field respectively taken at the inflection point marked by the arrow in Fig. 4.

The normalization procedure deserves a remark here. Namely, since the magnetic field dependence of both the

calculated M^* and LMR does not have "peculiar points" like maximums, the normalization have been performed in the corresponding inflection points. To determine the inflection point precisely, we first differentiate $\rho(B, T)$ over B , find the extremum of derivative and normalize the values of the function and the argument by their values in the inflection point. Then, both theoretical (shown by the solid line) and experimental (marked by the geometrical figures) curves have been normalized by their inflection points, which also reveal the universal behavior - the curves at different temperatures merge into single one in terms of the scaled variable y and show the scaling behavior over three decades in the normalized magnetic field.

The transition region at which LMR starts to decrease is shown in the inset to Fig. 1 by the hatched area. Obviously, as seen from Eq. (14), the width of the transition region being proportional to $B_M \simeq B_{inf}$ decreases as the temperature T_f is lowered. In the same way, the inflection point of LMR, generated by the inflection point of M^* shown in the inset to Fig. 1 by the arrow, shifts to lower B as T_f is decreased. All these observations are in excellent agreement with the facts [19].

D. Magnetic entropy

The evolution of the derivative of magnetic entropy $dS(B, T)/dB$ as a function of magnetic field B at fixed temperature T_f is of great importance since it allows us to study the scaling behavior of the derivative of the effective mass $TdM^*(B, T)/dB \propto dS(B, T)/dB$. While the scaling properties of the effective mass $M^*(B, T)$ can be analyzed via MLR as we have shown in Subsection C.

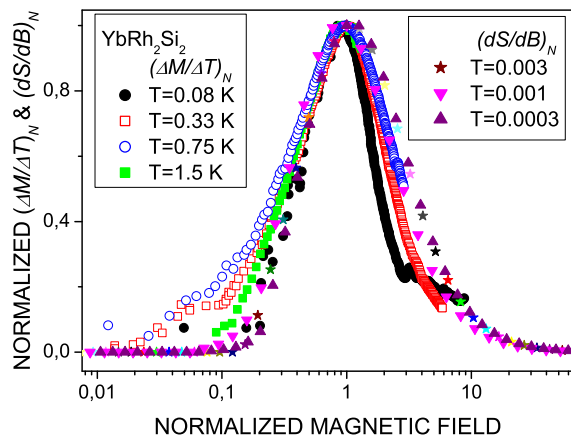


FIG. 5: Normalized magnetization difference divided by temperature increment $(\Delta M/\Delta T)_N$ vs normalized magnetic field at fixed temperatures (listed in the legend in the upper left corner) is extracted from the facts collected on YbRh_2Si_2 [20]. Our calculations of the normalized derivative $(dS/dB)_N \simeq (\Delta M/\Delta T)_N$ vs normalized magnetic field are given at fixed dimensionless temperatures T/μ (listed in the legend in the upper right corner). All the data are shown in the geometrical figures depicted in the legends.

As seen from the consideration in Subsection C and from Eqs. (11) and (14), at $y \leq 1$ the derivative $-dM_N(y)/dy \propto y$ with $y = (B - B_{c0})/(B_{inf} - B_{c0}) \propto (B - B_{c0})/T_f$. We recall that the effective mass as a function of B does not have the maximum, see Subsection C. At elevated y the derivative $-dM_N(y)/dy$ possesses a maximum at the inflection point and then becomes a diminishing function of y . Upon using the variable $y = (B - B_{c0})/T_f$, we conclude that at decreasing temperatures, the leading edge of the function $-dS/dB \propto -TdM^*/dB$ becomes steeper and its maximum at $(B_{inf} - B_{c0}) \propto T_f$ is higher. These observations are in quantitative agreement with striking measurements of the magnetization difference divided by temperature increment, $-\Delta M/\Delta T$, as a function of magnetic field at fixed temperatures T_f collected on YbRh_2Si_2 [20]. We note that according to the well-know thermodynamic equality $dM/dT = dS/dB$, and $\Delta M/\Delta T \simeq dS/dB$.

To carry out a quantitative analysis of the scaling behavior of $-dM^*(B, T)/dB$, we calculate as described above the entropy $S(B, T)$ as a function of B at fixed dimensionless temperatures T_f/μ shown in the upper right corner of Fig. 5. This figure reports the normalized $(dS/dB)_N$ as a function of the normalized magnetic field. The function $(dS/dB)_N$ is obtained by normalizing $(-dS/dB)$ by its maximum taking place at B_M , and the field B is scaled by B_M . The measurements of $-\Delta M/\Delta T$ are normalized in the same way and depicted in Fig. 5 as $(\Delta M/\Delta T)_N$ versus normalized field. It is seen from Fig. 5 that our calculations are in excellent agreement with the facts and both the experimental functions $(\Delta M/\Delta T)_N$ and the calculated $(dS/dB)_N$ ones show the scaling behavior over three decades in the normalized magnetic field.

V. SUMMARY

We have analyzed the non-Fermi liquid behavior of strongly correlated Fermi systems using the density functional theory of fermion condensation and derived equations for the effective mass of quasiparticles in both homogeneous systems and solids with a lattice, and showed that extended quasiparticles paradigm is strongly valid, while the dependence of the effective mass on temperature, number density, applied magnetic fields etc gives rise to the NFL behavior. The obtained results are illustrated with calculations of the thermodynamic and transport functions of strongly correlated Fermi-systems. Possible energy scales in these functions are discussed. We have demonstrated that our comprehensive theoretical study of the heat capacity, magnetization, energy scales, the longitudinal magnetoresistance and magnetic entropy are in good agreement with the outstanding recent facts collected on the HF metal YbRh_2Si_2 .

VI. ACKNOWLEDGEMENTS

This work was supported in part by the grants: RFBR No. 09-02-00056 and the Hebrew University Intramu-

ral Funds. VRS is grateful to the Lady Davis Foundation for supporting his visit to the Hebrew University of Jerusalem.

-
- [1] E.M. Lifshitz, L.P. Pitaevskii, *Statistical Physics, Part 2*, Butterworth-Heinemann, Oxford, 1999.
 - [2] T. Senthil, M. Vojta, S. Sachdev, *Phys. Rev. B* 69 (2004) 035111.
 - [3] P. Coleman, A.J. Schofield, *Nature* 433 (2005) 226.
 - [4] H.v. Löhneysen, A. Rosch, M. Vojta, P. Wölfle, *Rev. Mod. Phys.* 79 (2007) 1015.
 - [5] P. Gegenwart, Q. Si, F. Steglich, *Nature Phys.*, 4 (2008) 186.
 - [6] S. Sachdev, *Nature Phys.* 4 (2008) 173.
 - [7] V.A. Khodel, V.R. Shaginyan, *JETP Lett.* 51 (1990) 553.
 - [8] M. Ya. Amusia, V.R. Shaginyan, *Phys. Rev. B* 63 (2001) 224507.
 - [9] G.E. Volovik, *Springer Lecture Notes in Physics* 718 (2007) 31.
 - [10] V.R. Shaginyan, M.Ya. Amusia, K.G. Popov, *Physics-Uspokhi* 50 (2007) 563.
 - [11] V.A. Khodel, J.W. Clark, M.V. Zverev, *Phys. Rev. B* 78 (2008) 075120.
 - [12] J. Dukelsky, et. al., *Z. Phys. B: Condens. Matter* 102 (1997) 245.
 - [13] J.W. Clark, V.A. Khodel, M.V. Zverev *Phys. Rev. B* 71 (2005) 012401.
 - [14] V.R. Shaginyan, et. al., *Europhys. Lett.* 76 (2006) 898.
 - [15] V.R. Shaginyan, K.G. Popov, V.A. Stephanovich, *Europhys. Lett.* 79 (2007) 47001.
 - [16] V.R. Shaginyan, A. Z. Msezane, K. G. Popov, and V. A. Stephanovich, *Phys. Rev. Lett.* 100 (2008) 096406.
 - [17] V.R. Shaginyan, *Phys. Lett. A* 249, 237 (1998).
 - [18] N. Oeschler, et. al., *Physica B* 403 (2008) 1254.
 - [19] P. Gegenwart, et. al., *Science* 315 (2007) 969.
 - [20] Y. Tokiwa, et. al., *Phys. Rev. Lett.* 102 (2009) 066401.
 - [21] M. Pfizner, P. Wölfle, *Phys. Rev. B* 33 (1986) 2003; D. Wollhardt, P. Wölfle, P.W. Anderson, *Phys. Rev. B* 35 (1987) 6703.
 - [22] L.N. Oliveira, E.K.U. Gross, W. Kohn, *Phys. Rev. Lett.* 60 (1988) 2430.
 - [23] K. Kadowaki, S.B. Woods, *Solid State Commun.* 58 (1986) 507.
 - [24] A. Khodel, P. Schuck, *Z. Phys. B: Condens. Matter* 104 (1997) 505.
 - [25] V.R. Shaginyan, M.Ya. Amusia, A.Z. Msezane, K.G. Popov, V.A. Stephanovich, *Phys. Lett. A* 373, (2009) 986.